CONFERENCE PROCEEDINGS

Numerical analysis of pilot test plume evolution patterns using two different equations-of-state

Weon Shik Han, New Mexico Institute of Mining and Technology
Brian McPherson, New Mexico institute of Mining and Technology
Rajesh Pawar, Los Alamos National Laboratory,
Jason Heath, New Mexico Institute of Mining and Technology

FOURTH ANNUAL CONFERENCE ON CARBON CAPTURE AND SEQUESTRATION DOE/NETL
May 2-5, 2005

Abstract

For geologic sequestration, an accurate equation of state (EOS) is critical for the evaluation and estimation of CO_2 migration and evolution patterns. We assembled and compared two different EOS algorithms – the Modified Redlich-Kwong (MRK) EOS and Span Wagner's EOS (SW). The MRK EOS employs modification of the van der Waals equations, while the SW EOS utilizes an empirical representation of the fundamental equation of Helmholtz energy. In this study, the developed codes were tested by simulating 1D core scale test and an actual pilot test in the West Pearl Queen reservoir near Hobbs, NM.

The TOUGH2 simulator was adapted to include these different equations of state algorithms. The modified simulator calculates the thermodynamic behavior of CO_2, water, and their mixtures (CO_2/H_2O). 1D core scale simulation results shows that different EOS algorithms can affect CO_2 migration rates very differently. The field-scale Queen Reservoir simulation captures special multiphase behavior including gravitational segregation, buoyancy driven flow, and solubility trapping. Plume evolution patterns exhibit three different stages such as the injection stage (1yr), force balance stage (1,000yr), and finally gravitational segregation stage (10,000yr). Following a lapse of 10,000 yrs (gravitational segregation stage), the supercritical CO_2 is converted the dissolved phase throughout the pilot test reservoir and the saturation ratio of supercritical CO_2 approaches zero, leading to the complete solubility trapping. Maximum CO_2 mass discrepancy by MRK EOSCO2 and SW EOSCO2 was 305 tons, which was around 15% of the total injected CO_2 (2083 tons) in the West Pearl Queen reservoir model. In addition to the difference of calculated CO_2 mass, the time occurring complete solubility mechanisms was, respectively, 7000 yr and 3000 yr by MRK EOSCO2 and SW EOSCO2.

1. Introduction

Concern about increasing concentration of carbon dioxide (CO_2) in the atmosphere has led to consideration of large-scale storage of anthropogenic CO_2 in the subsurface, including oil and gas reservoirs, deep saline aquifers, and coal beds. Bachu (2000) and Orr (2004) reviewed options for storing CO_2 in geologic formations and outlined advantages and disadvantages of each approach. CO_2 can be sequestered in geologic formations by three mechanisms (Hitchon, 1996). First, CO_2 can be trapped as separate phase (gas or supercritical fluid) under a low-permeability caprock, also called hydrodynamic trapping. Second, CO_2 can dissolve in groundwater, referred to as solubility trapping. This mechanism can increase the acidity of groundwater and affect the solubilities of minerals composing the host rock and caprock matrix. Third, CO_2 can react directly or indirectly with aquifer minerals and organic matter in geologic formations, leading to precipitation of secondary carbonate minerals and storage as a solid. This process is called mineral trapping. Fig. 1 shows several physical and chemical processes that can result in the long-term sequestration.

The following sections discuss pertinent processes and critical sequestration aspects schematically depicted in Fig. 1.

(a) Gravitational segregation

When supercritical CO_2 is injected, some of it will dissolve into the groundwater and the rest will remain as a separate phase, which will override the groundwater phase due to buoyancy forces (Law and Bachu, 1996). In general, dissolution of CO_2 in water increases the density of the aqueous mixture (CO_2/H_2O), causing gravitational segregation (or sinking) of the mixed phase (Fig. 1(A)). However, hydraulic gradients in the basin may cause migration of the dissolved phase with ambient formation water.

(b) Buoyancy driven over-ride

Unlike the dissolved CO_2 phase, a supercritical CO_2 plume will tend to float because density of the injected supercritical CO_2 is lighter than surrounding fluids (Fig. 1(B)). In addition to the density effect, the interfacial tension between supercritical CO_2 and water at typical reservoir conditions is very small. The combined effects of density (buoyancy) and interfacial tension are more dominant than capillary forces.

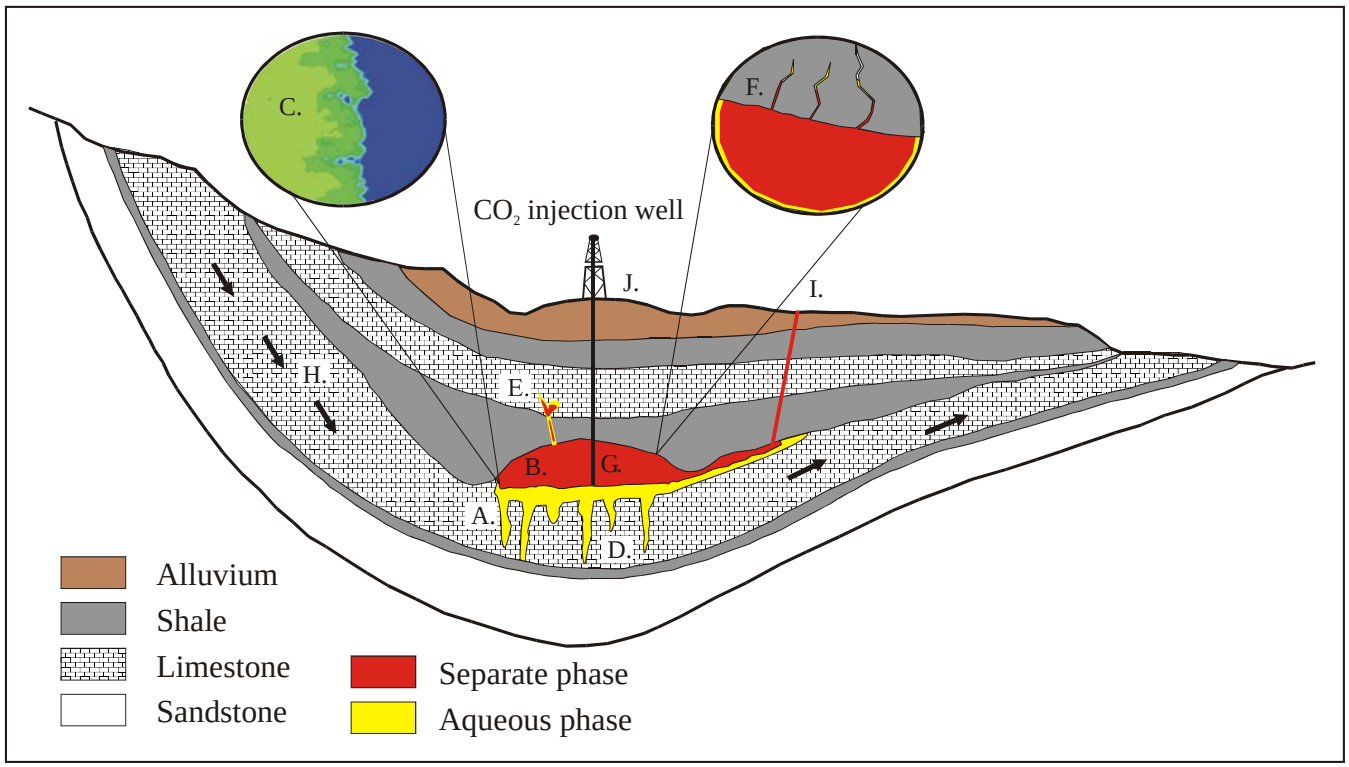

Fig. 1. Diagrammatic representation of relevant processes related to CO_2 sequestration: (a) gravitational segregation, (b) buoyancy driven over-ride, (c) viscous fingering, (d) phase partitioning, (e) chemical reaction (dissolution/precipitation), (f) seal integrity, (g) well injectivity, (h) groundwater flow direction and velocity, (i) surface leakage, (j) surface deformation

(c) Viscous Fingering

CO_2 sequestration in saline aquifers usually involves immiscible displacement of the brine phase by a less dense and less viscous separate CO_2 phase (Fig. 1(C)) (Garcia, 2003). Even though viscous fingering has been extensively studied in oil migration studies, research about viscous fingering effects of injected supercritical CO_2 is still immature.

(d) Phase Partitioning

The amount of dissolved CO_2 usually triggers a pH change of an aqueous system (Fig. 1(D)). To predict CO_2 partitioning with brine, an accurate equation of state (EOS) is necessary. Using experimental data for comparison, EOS algorithms can predict CO_2 solubility in brine reasonably well (Duan and Sun, 2003). However, several limitations still exist. First, most available CO_2 solubility data are derived from experimental work on the NaCl-H_2O-CO_2 system rather than natural brines that are more compositionally complex. Second, most EOS algorithms are based on binary sets of data, including data at low pressures and temperatures and data at high pressures and temperatures, respectively. Finally, mathematical formulations of EOS are computationally demanding, making application in numerical simulation impractical (Garcia, 2003).

(e) Chemical reaction

One of the most important considerations is chemical reaction that alters permeability and porosity of the aquifer matrix (Fig. 1(E)). For example, carbonate dissolution is sufficiently fast enough to be an equilibrium reaction. Thus, this reaction may alter well injectivity by increasing porosity and permeability near the injection well. In contrast, some altered mineral products such as clay minerals will decrease porosity and permeability and degrade well injectivity. Unlike equilibrium reactions, some kinetic reactions are too slow to investigate in the laboratory or during in-situ injection experiments. These kinetic reactions may occur continuously long after CO_2 injection activity stops.

(f) Seal integrity

Seal integrity is critical for long-term containment of CO_2 after injection (Fig. 1(F)). High pressures induced by CO_2 injection may cause fractures in the sealing unit. Chemical reactions (precipitation) may seal fractures, however. The complex evolution of chemical composition and stress field of fractured flow will determine the long-term effectiveness of sealing layers.

(g) Well injectivity

Well injectivity is a term applied to plugging and formation damage and associated changes in injection well performance (Saripalli *et al*, 2000) (Fig. 1(G)). From results of reactive transport modeling and field data analysis, Xu *et al*., (2004) concluded that reductions of porosity and permeability by significant precipitation of amorphous silica could cause the injectivity loss within a 10 m radius from the injection well.

(h) Groundwater flow and water chemistry

Advective groundwater flow is dominant in sedimentary basins (Fig. 1(H)). In basin environments, groundwater velocity may be faster than chemical reaction rates. Because of the short time that groundwater and minerals are typically in contact, the chemical compositions of groundwater may show undersaturation of relevant minerals. However, diffusive flow may dominate in certain locations such as shale and clay layers. In these cases, diffusive flow may be slower than the reaction rate and the chemical composition of groundwater may show supersaturation of relevant minerals. These effects may be characterized in many ways, e.g., the Damkohler number.

(i) Surface leakage

A caprock may be discontinuous and may contain imperfections such as faults and fractures of various sizes (Fig. 1(I)). These undiscovered geologic features could become leakage pathways. Furthermore, the hydraulic properties of a fault may change with CO_2 injection pressure (Rutqvist and Tsang, 2002).

(j) Surface deformation

Underground injection of compressed CO_2 can cause extreme fluid pressures and expansion of subsurface units, leading to expressed deformation at the surface (Fig. 1(J)). In addition to surface deformation, the increased pore pressure will change the stress field of aquifer and may cause deformation of rock matrix.

2. Objective

The objective of this research is to investigate plume evolution patterns using two fundamentally different equations of states (MRK EOSCO2 and SW EOSCO2). EOSs, which thermodynamically calculate how much separate CO_2 is partitioned into aqueous CO_2, can be critical to predict the reservoir capacity and solubility trapping mechanisms. Moreover, migration rate of CO_2 plume might strongly depend on density and viscosity, which is calculated from EOSs subroutine. Thus, this work includes improving the current understanding of mechanisms associated with CO_2 migration rate and CO_2 partitioning predicted from two different EOSs. In addition, the buoyancy driven force, gravitational segregation, and solubility trapping mechanism are especially evaluated among the above listed pertinent processes of CO_2 sequestration.

3. Approach

Numerical simulation of CO_2 sequestration requires the realistic representations of the thermodynamic properties (density, fugacity, enthalpy, viscosity) of water, separate phase CO_2 (gas and supercritical phases), and aqueous mixtures of CO_2 over the range of temperatures and pressures anticipated in a given geologic setting. In addition, capillary pressure and relative permeability must be evaluated. Subsequently, an adequate representation of the solubility of CO_2 as a function of temperature and pressure needs to be included.

We have assembled and compared two EOS algorithms (Fig. 2). One is the modified Redlich-Kwong (MRK) EOSCO2 that employs modification of the attractive term from van der Waals equation (Kerrick and Jacobs, 1981; Weir *et al*, 1996; Cole, 2000). The other is Span and Wagner (SW) EOSCO2, an empirical representation of the fundamental equation of Helmholtz energy (Span and Wagner, 1996).

Only Specific density, fugacity coefficient, and specific enthalpy among the thermodynamic properties were calculated from Modified Redlich-Kwang EOS in MRK EOSCO2 and same thermodynamic properties were from Span and Wager EOS in SW EOSCO2 (Fig. 2). The thermodynamic properties from Span and Wagner (1996), accurate within 0.05% over P-T range of our research interest including the near-critical region, are almost identical to IUPAC data sets. In addition to the accuracy, Span and Wagner EOS is available to the wider range (P: 0.1MPa-800MPa, T: 273.15K and 800K) compared to modified Redlich-Kwang EOS (P: 1MPa-100MPa and T: 288.15K-623.15K). However, the actual modeling capability of EOSs mainly depend on the solubility EOS because the predictable ranges by solubility EOS is normally less than those by density, fugacity coefficient, and enthalpy EOSs. The solubility EOS was adapted from Reid et al (1987) in MRK EOSCO2 and from Diamond and Akinfiev (2003) in SW EOSCO2 (Fig. 2). The actual range, which depends on the solubility EOS, of these integrated EOS algorithms are, respectively, 1MPa-45MPa and 288.15K-373.15K in MRK EOSCO2 and 0.1MPa-100MPa and 273.15K-373.15K in SW EOSCO2.

Both EOS algorithms and sources were designed for the TOUGH2 simulator, which includes coupled flow of heat and groundwater flow (Pruess, 1991).

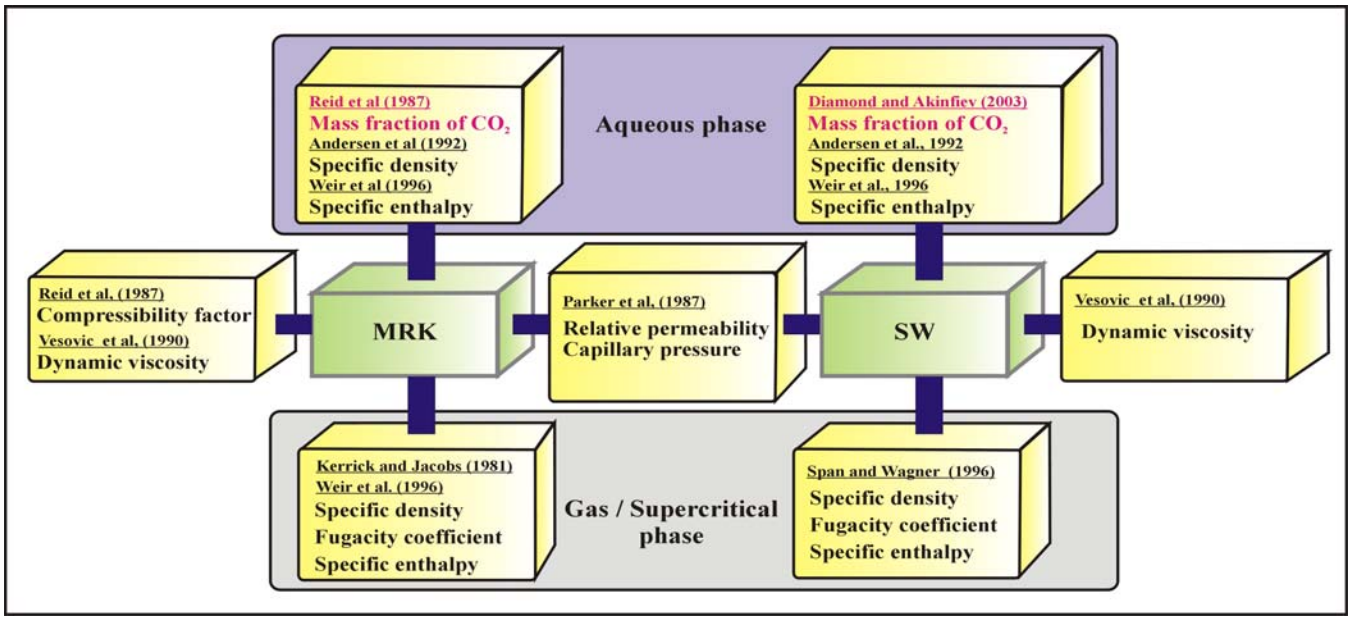

Fig. 2. The schematic diagram of MRK EOSCO2 and SW EOSCO2

4. Results and applications

4.1. Equation of State (EOS)

This section summarizes the inter-relationship used to calculate individual thermophysical properties of pure CO_2 and CO_2/H_2O mixture system. Explanation of pure H_2O properties does not included. Fig. 3 shows the interrelationship of the individual thermophysical properties in both MRK EOSCO2 and SW EOSCO2.

In general, dependent variables of EOSs are not pressure and temperature because choosing both pressure and temperature as dependent variables make calculation of EOS difficult near the critical point. Although there exist problems in choosing pressure and temperature as dependent variables, it is almost necessary to select pressure and temperature as dependent variables in deep reservoir simulation because the estimation of the density values as an input parameter is practically difficult due to the profile of the density variation not being linear. Thus, the numerical method was used to switch the original primary variables (SW EOSCO2: density and temperature, MRK EOSCO2: molal volume and temperature). The gray box shows the location where the primary variables are switched in Fig. 3.

The arrows indicate the direction of the input parameters to calculate thermophysical properties (Fig. 3). For example, the arrows from temperature and pressure boxes converge into CO_2 density (gas/supercritical phase) box in Fig.3(a). This indicates that the calculation of CO_2 density requires pressure and temperature as dependent variables. For another example, the arrows from pressure, temperature, saturation pressure of water, fugacity coefficient of CO_2, fugacity coefficient of water, and water density boxes converge the mole fraction (aqueous CO_2) box in Fig.3(a). This also indicates that the calculation of mole fraction requires pressure, temperature, saturation pressure of water, fugacity coefficient of CO_2, fugacity coefficient of water, and water density as dependent variables. Above examples show how individual thermophysical properties are closely interrelated in EOS algorithms.

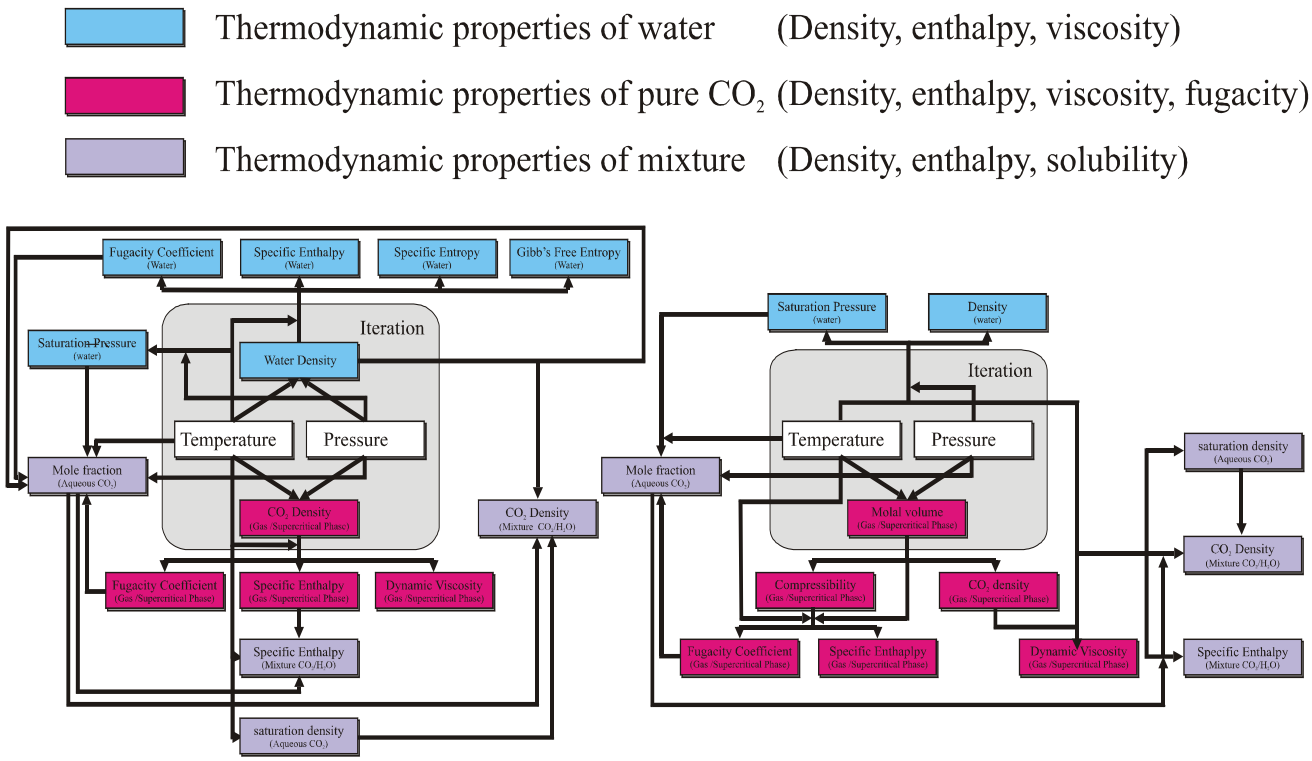

(a) SW EOSCO2 (b) MRK EOSCO2

Fig. 3. The schematic representation of MRK EOSCO2 and SW EOSCO2 algorithms (Blue boxes: thermodynamic properties of water, Red boxes: thermodynamic properties of pure CO_2, and Purple boxes: thermodynamic properties of mixture (CO_2/H_2O))

Values for the fugacity coefficient of CO_2 predicted from MRK EOSCO2 appear to be systematically lower than those from IUPAC and SW EOSCO2 (Fig. 4(a)). Solving for mole fraction of gaseous solute generally requires Henry's relation, which needs the fugacity coefficient as a dependent variable. Because of the lower prediction of the fugacity coefficients, mole fraction from MRK EOSCO2 does not provide a good fit with solubility data (Fig. 4(c)). In other words, the calculation of mole fraction in MRK EOSCO2 requires pressure, temperature, saturation pressure of water, and fugacity coefficient of CO_2 as dependent variables (Fig. 3(b)). The lower predicted fugacity coefficients from MRK EOSCO2 affect the calculated values of mole fractions even though the solubility algorithm is correct. Finally, thermophysical properties both CO_2 density (mixture CO_2/H_2O) and specific enthalpy (mixture CO_2/H_2O) from MRK EOSCO2, which adapt mole fraction as an input parameter, show the discrepancy with those from SW EOSCO2 (Fig. 4(b)).

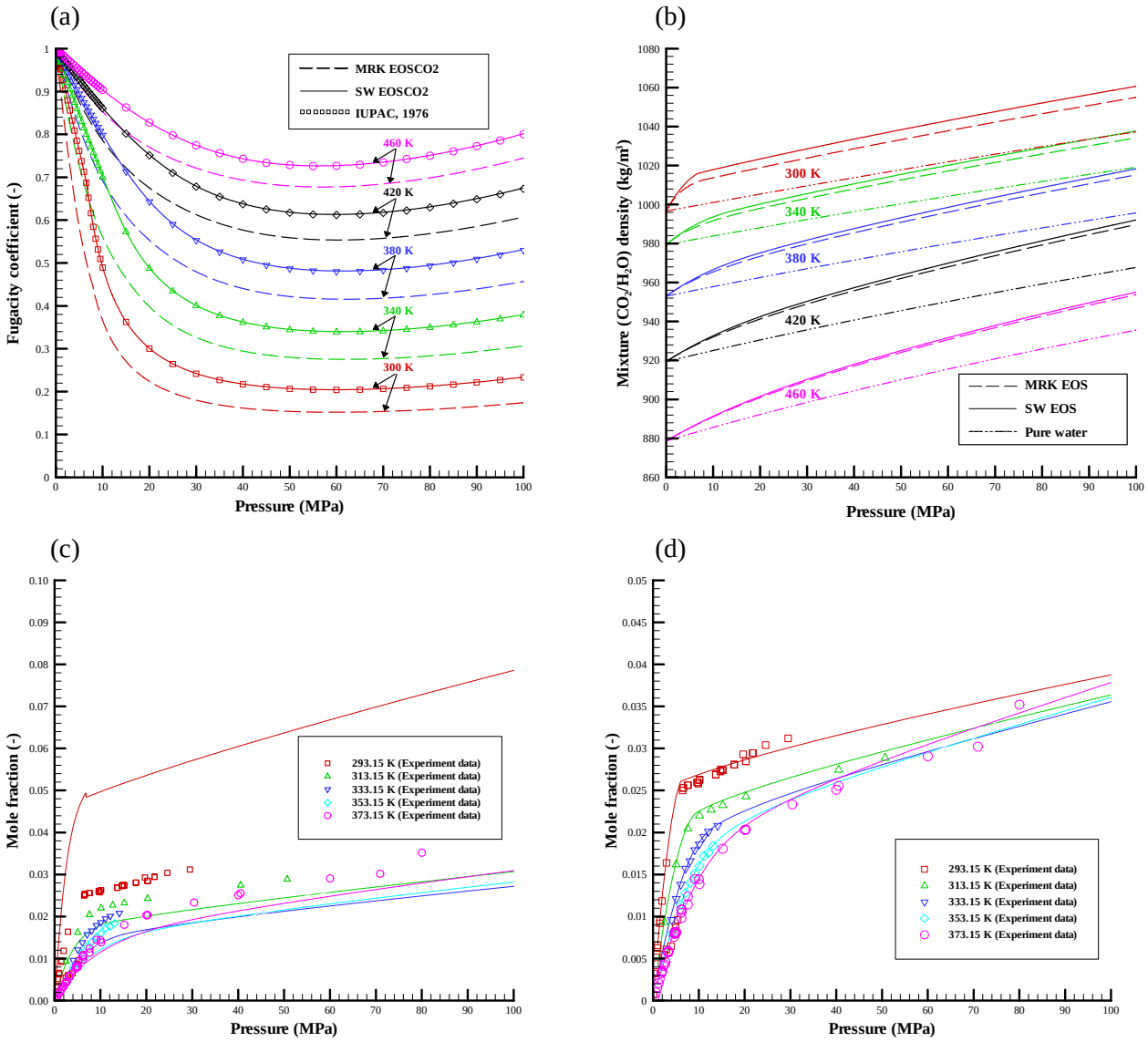

Fig. 4. Thermodynamic properties for pure CO_2 as a function of pressure along several representative isotherms. IUPAC refers to values tabulated in Angus et al., 1976 ((a) fugacity coefficient for pure CO2; (b) density of aqueous mixture (CO_2/H_2O) (c) solubility of pure CO_2 in pure water using MRK EOSCO2; (d) solubility of pure CO_2 in pure water using SW EOSCO2)

In detail, Fig. 4(c) illustrates that the MRK EOSCO2 overestimates the solubility values below 30°C (303.15K) and underestimates those over 30°C (303.15K). The adequate condition for storing CO_2 as a separate phase requires above critical temperature (about 31°C) and pressure (about 7.38 MPa). The condition for supercritical CO_2 state would be roughly met for depth greater than 750 m. Thus, at this condition, solubilities predicted by MRK EOSCO2 will be underestimated.

Although Span and Wagner algorithm predicts the most accurate CO_2 thermodynamic properties (density, fugacity coefficient, and enthalpy) and the wider range, the modified Redlich-Kwong (MRK) EOS is easy to code and modify so that many researchers still actively use it. Spycher et al (2003) developed their own version of MRK EOS to predict the fugacity coefficients and solubility of CO_2 in pure water. By adjusting the attractive term, their EOS (<2%) can predict CO_2 solubility with success from 12°C (285.15K) to 100°C (373.15K) and up to 60MPa.

4.2. CO_2 migration simulation: 1D core scale model

Individual phase flux, aqueous CO_2 and separate CO_2, are calculated by a multiphase version of Darcy's law.

$$F = \rho\upsilon = -k\frac{k_r\rho}{\mu}(\nabla P - \rho g) \qquad \text{(Eq.1)}$$

The individual phase flux in a multiphase version of Darcy's law is linearly dependent on the fluid density and reversibly on the fluid viscosity if rock permeability and relative permeability of phase are consistent. We used a same relative permeability function in both MRK EOSCO2 and SW EOSCO2 (Parker *et al.*, 1987). Because the calculation of relative permeability does not require any thermodynamic properties of CO_2 and CO_2/H_2O mixture, the relative permeability calculated by both MRK EOSCO2 and SW EOSCO2 are same. In addition, the entire model was assigned by same permeability ($10^{-14}m^2$). Thus, the individual phase flux only depends on fluid density and viscosity.

Because few viscosity equations of state for CO_2/H_2O mixture exist and available data suggest that the viscosity of pure water is not significantly affected by the presence of dissolved CO_2, the viscosity of pure water predicted from the relationship provided by the International Steam Tables have been used to represent the viscosity of aqueous mixture of CO_2 (International formulation Committee, 1967). Finally, the individual mass flux is only dependent on density because viscosity values predicted by MRK EOSCO2 and SW EOSCO2 are same.

1D laboratory core scale model was developed to investigate how the migration rate of aqueous CO_2 is dependent on density between MRK EOSCO2 and SW EOSCO2. The 100 cells model (0.8 m) was generated (Fig. 5(a)). The temperature was assigned 38°C (311.15 K) in the entire model and constant head boundaries were assigned at upper (20MPa) and bottom (18MPa) boundary. The injection rate of CO_2 was 10^{-5} kg/s during 1 day. Breakthough curves at three time steps are provided in Fig. 5(b).

First, mass fraction values of aqueous CO_2 predicted by MRK EOSCO2 are clearly less than those by SW EOSCO2 because temperature is 38 °C (311.15 K) in the entire model (Fig. 5(b)). Second, the peaks of curves calculated by MRK EOSCO2 migrate little behind. As mentioned before, the individual mass flux in a multiphase version of Darcy's law is linearly dependent on the fluid density when rock permeability, relative permeability of phase, and viscosity are fixed. From the mixture density plot in Fig. 4(b), mixture density by MRK EOSCO2 is little smaller than that by SW EOSCO2 at around 38 °C (311.15 K). The underestimation of mixture density by MRK EOSCO2 make CO_2 migration rate slow. However, as temperature increase, the discrepancy of mixture density from both MRK EOSCO2 and SW EOSCO2 is getting decreased (Fig. 4(b)). Thus, the CO_2 flux rate is going to be similar as temperature increases.

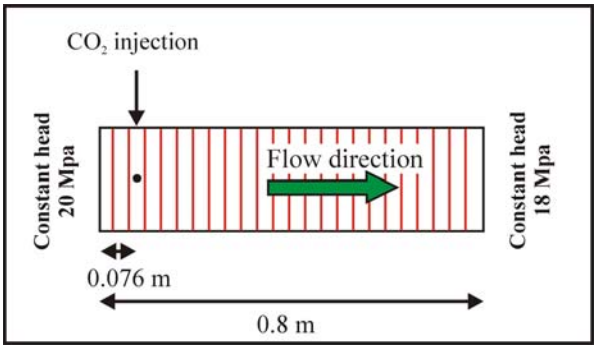

(a)

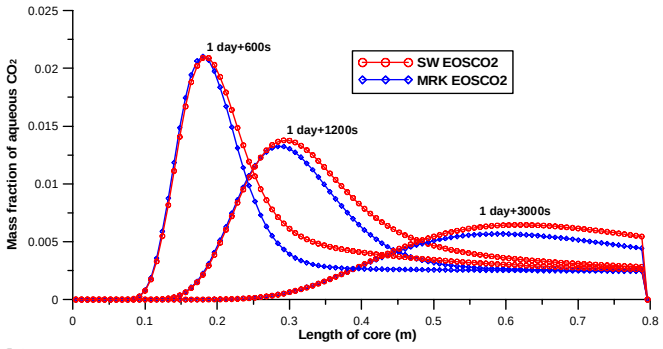

(b)

Fig. 5. 1D laboratory core model to investigate CO_2 migration rate. (a) 1D laboratory core model, (b) mass fraction of aqueous CO_2 versus distance into the column at three time steps.

Obviously, the flux rate of separate CO_2 is also affected by the density and viscosity values. The density of separate CO_2 by MRK EOSCO2 and SW EOSCO2 are almost identical (Figure is not addressed in this paper). Viscosity calculation of separate CO_2 requires density of CO_2 and temperature as dependent variables (Fig. 3)

(Vesovic et al. 1990). Because the input values, the density of CO_2 and temperature, are same at both MRK EOSCO2 and SW EOSCO2, the predicted viscosity of separate CO_2 is also identical. Thus, the migration rate of separate CO_2 does not show any discrepancy.

4.3. CO_2 plume evolutionary patterns simulation: West Pearl Queen reservoir

The goal of developing this simulation is to compare the discrepancy of CO_2 mass fraction predicted from these two EOSs (MRK EOSCO2 and SW EOSCO2) and to reconstruct a micro pilot scale CO_2 sequestration experiment at West Pearl Queen reservoir in southwest New Mexico. The West Pearl Queen reservoir was targeted as a potential experiment site for a CO_2 pilot injection study (Fig. 6). In field experiment, about 2090 tons of CO_2 were injected during 53 days from December 20, 2002 to February 10, 2003 (Pawar *et al*., 2003). Laboratory CO_2 flood tests were previously conducted by the New Mexico Petroleum Recovery Research Center to characterize core scale flow and transport of CO_2 (Krumhansl *et al*., 2002). In addition to the laboratory CO_2 flood test, numerical flow and transport simulations for the West Pearl Queen reservoir pilot injection test were developed using the commercial simulator ECLIPSE (Pawar *et al*. 2003). In this exercise, TOUGH2 simulator, which was the numerical simulator for multi-dimensional fluid and heat flow, and the developed two CO_2 equations of state (MRK EOSCO2 and SW EOSCO2) were used for this modeling effort.

The model was composed of 6000 grid blocks (30 x 200) and three different layers, which were Severn River formation, Shattuck sandstone, and Lower Queen formation. The size of individual cell was 2 m x 7.5 m. The assigned boundary conditions, CO_2 injection depth, and thickness of formations are provided in Fig. 6. Among the several model input parameters, the permeability and porosity values in the model were based on core flood experiment (Aabel, 2005). CO_2 injection rate was 39312 kg/day during 53 days in the model. This total amount (2083.536 tons) of injected CO_2 is compatible to the amount (around 2090 tons) of actual field injection. A detailed description of the model input parameters is listed in Table 1.

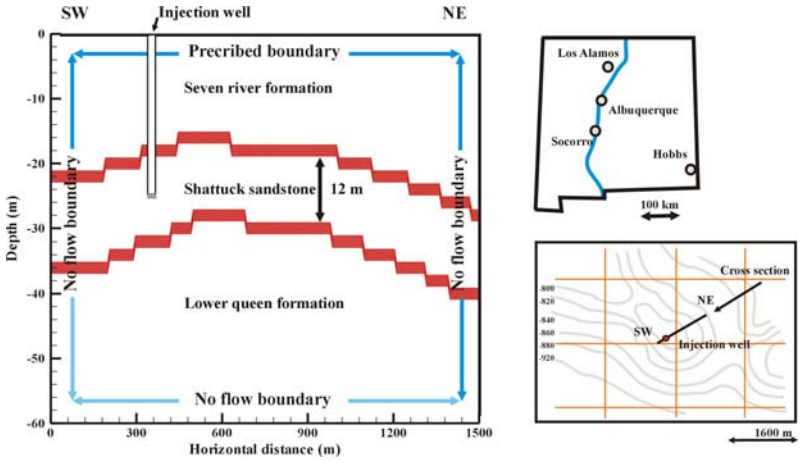

Fig. 6. Model description of experimental pilot test area in West Pearl Queen reservoir. Vertical exaggeration is 25 times.

Table 1. Model input parameters description

	Seven river formation	Shattuck sandstone	Lower queen formation
Porosity	0.05	0.15	0.05
Horizontal perm. (m^2)	2.0^{-15}	6.12^{-14}	2.0^{-15}
Vertical perm. (m^2)	2.0^{-17}	6.12^{-16}	2.0^{-17}
Temperature gradient	Top: 44°C	Bottom: 46°C	0.03°C/10 m
Pressure gradient	Top: 8.0 MPa	Bottom: 8.7 MPa	* hydrostatic pressure
Injection	39312 kg/day during 53 days		

The temperature range from top to bottom boundary in this model was approximately between 44°C (317.15K) and 46°C (319.15K). From the CO_2 solubility description in Fig. 4(c), MRK EOSCO2 overestimated the values of CO_2 solubility below 30°C and underestimated those above 30°C. In this West Pearl Queen reservoir simulation, MRK EOSCO2 underestimates the values of CO_2 solubility because the temperature profile of the West Pearl Queen reservoir model is greater than 30°C. The plume evolution patterns of aqueous CO_2 from both MRK EOSCO2 and SW EOSCO2 clearly indicate this discrepancy that MRK EOSCO2 underestimates CO_2 solubility (Fig. 7).

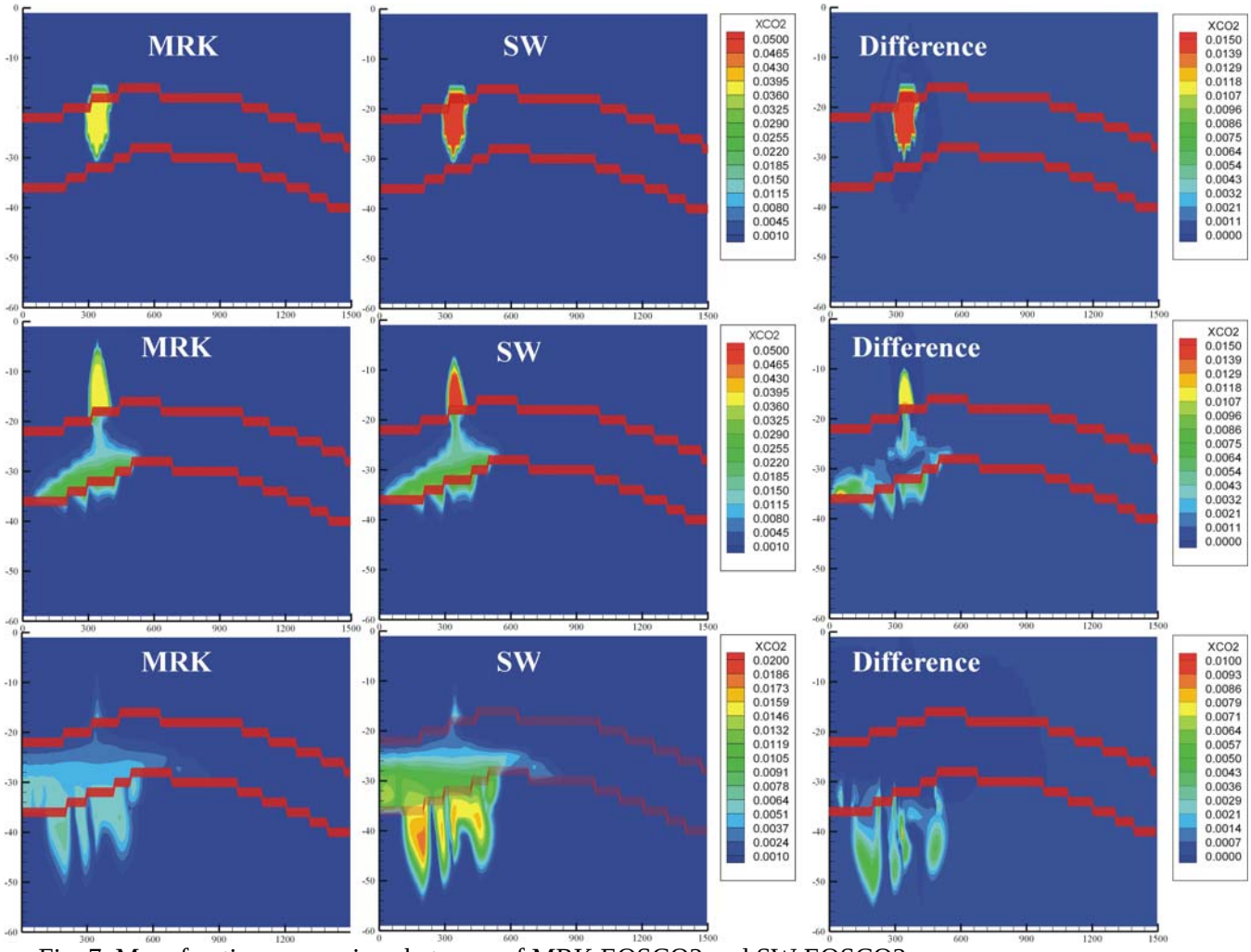

Fig. 7. Mass fraction comparison between of MRK EOSCO2 and SW EOSCO2.

The simulation results of plume evolution patterns, which explain the distribution of mass fraction of dissolved CO_2 and saturation of separate CO_2, were plotted at 1, 1,000, and 10,000 yrs (Fig. 8). The red lines are the upper and bottom boundary of Shattuck sandstone.

Fig. 8(a) illustrates the injection stage (1yr) when aqueous and separate CO_2 plumes expand from the injection well. At 1000 yr, distinct partitioning of aqueous phase CO_2 is shown in the middle of the Shattuck sandstone layer (Fig. 8(b)). In addition to the distinct partitioning of aqueous phase CO_2, the plume of separate phase CO_2 at 1000 yr flows upward compared to that at 1 yr due to the buoyancy driven force. Thus, the center of separate CO_2 plume is located above the Shattuck sandstone's upper boundary at 1000 yr. However, aqueous phase CO_2 (mixture of CO_2/H_2O) is accumulated on the top of the Shattuck sandstone's lower boundary and does not gravitationally segregate into the Lower Queen formation because vertical permeability (2.0^{-17} m^2) of the Lower Queen formation is smaller than that (6.12^{-16} m^2) of the Shattuck sandstone. The accumulation of CO_2 plume above the low permeability formation indicates that permeability is an important factor controlling the migration

of CO_2 plume. A certain amount of aqueous CO_2 migrates upward despite of the greater density (Fig. 8(b)). This is because the supercritical CO_2 phase flows upward by buoyancy driven force and supercritical CO_2 is simultaneously converted into dissolved phase. Subsequently, gravitational segregation gradually occurs because the mixture density of CO_2/H_2O is heavier than the surrounding fluid.

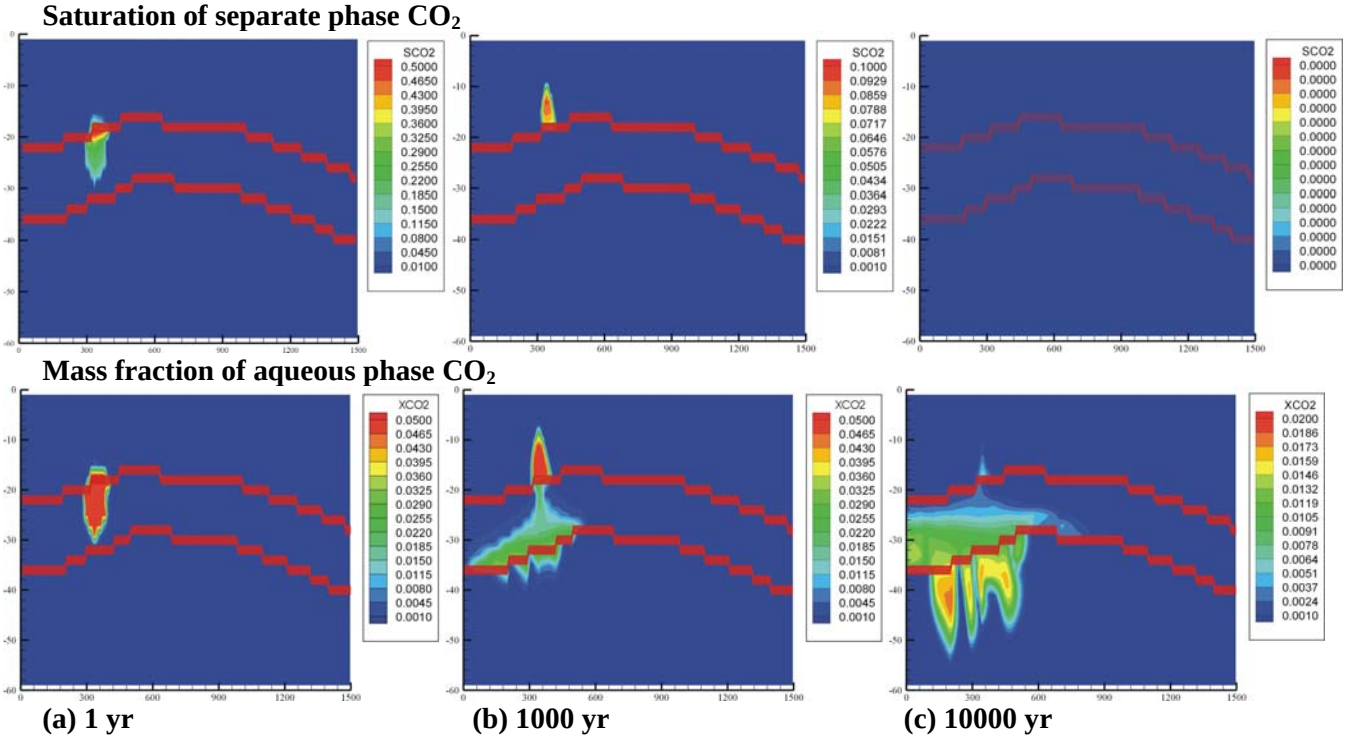

Fig. 8. Evolution of mass fraction of aqueous phase CO_2: (a) injection stage (1 yr), (b) force balance stage between buoyancy and gravitational segregation (1,000 yr), (c) gravitational segregation stage (10,000 yr).

After a lapse of 10,000 yrs, all of separate phase CO_2 is converted into the dissolved phase. Much of the CO_2 is trapped as a dissolved phase, called "solubility trapping" (Fig. 8(c)). Simulation results suggest that significant amounts of CO_2 are stored as a dissolved phase into fluid after a long geologic time period. Phase conversion from separate phase into dissolved phase will mainly depend on pressure, temperature, and salinity of formation water that control the CO_2 solubility in fluid.

CO_2 mass partitioning plots provide the useful method to quantify how much CO_2 are stored as a form of aqueous phase and as a form of separate phase from both MRK EOSCO2 and SW EOSCO2 (Fig. 9(a)). The amount of total injected CO_2 is 2083 tons during 53 days in this simulation. After starting the injection activity, separate CO_2 increased and simultaneously convert into aqueous phase. Thus, the amount of both separate CO_2 and aqueous CO_2 increase at the same time during 53 days (Fig. 9(a)). After stopping CO_2 injection at 53 days, the amount of separate CO_2 suddenly drop because of the phase conversion from separate CO_2 to aqueous CO_2.

There are critical discrepancies of CO_2 mass predicted by SW EOSCO2 and MRK EOSCO2. The mass of aqueous CO_2 predicted by MRK EOSCO2 is lower than those by SW EOSCO2 (Fig. 9(a)). This result is coincident with the previous results, which MRK EOSCO2 underestimate the solubilities over 30°C (Fig. 4(c)). In reverse, the mass of separate CO_2 by MRK EOSCO2 is greater than those by SW EOSCO2 because the total injected CO_2 is equal to the sum of aqueous CO_2 and separate CO_2.

The difference of mass fraction is small between MRK EOSCO2 and SW EOSCO2 (Fig. 7). However, the actual mass of CO_2 in the entire model by MRK EOSCO2 and SW EOSCO2 are markedly different (Fig. 9(b)). Figure 9(b) shows the absolute values, calculated by subtracting MRK EOSCO2 from SW EOSCO2 in either aqueous CO_2 or separate CO_2. The maximum difference value is 305 tons at 200 yr. The 305 tons is 15 % of the total injected CO_2 (2083 tons). This result clearly indicates how the equation of state plays an important role in

CO_2 sequestration simulation analysis, especially estimates of long-term migration patterns. Even though the solubility discrepancy by MRK EOSCO2 and SW EOSCO2 is small in Fig. 4(c), the difference of mass CO_2 in the entire model is enormously increased.

The EOS used for a given study also strongly affects the time when all of separate CO_2 change into aqueous CO_2. All of separate CO_2 convert into aqueous CO_2 after 3000 yr by SW EOSCO2. Thus, complete solubility trapping mechanisms is done after 3000 yrs. However, MRK EOSCO2 requires 7000 yr to store CO_2 as a complete solubility trapping mechanism.

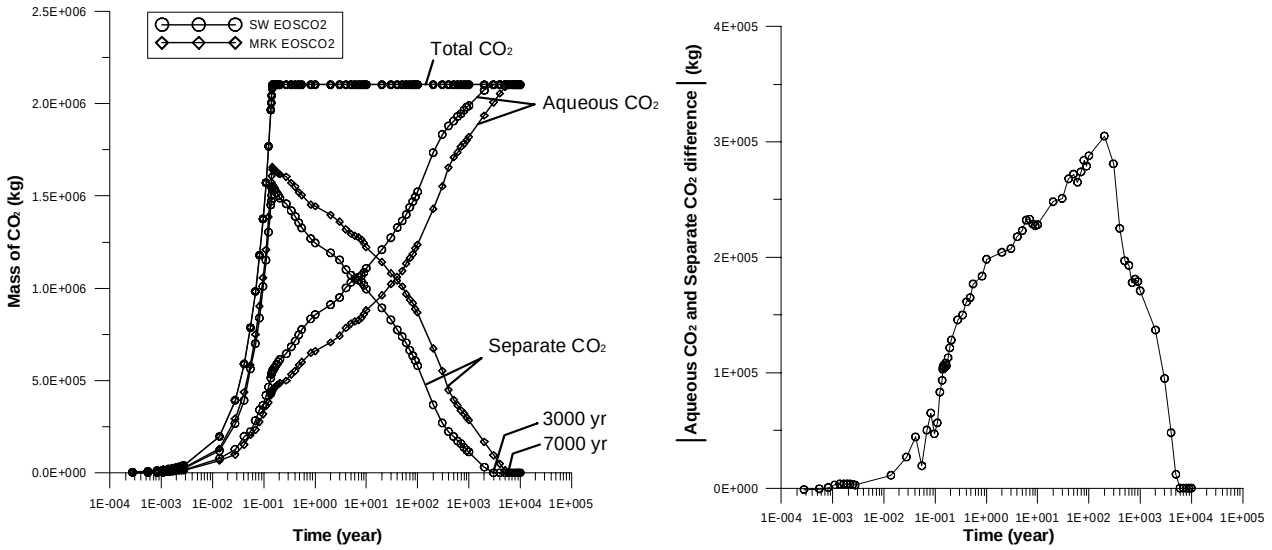

(a) (b)

Fig. 9. (a) CO_2 mass partitioning between aqueous and separate phase and total mass of injected CO_2, (b) the absolute values of the difference between MRK EOSCO2 and SW EOSCO2.

The relationship for the solubility of CO_2 in this work was derived for pure water. However, most reservoirs below depths of a few hundred meters contain saline formation water. Increasing salinity of water decreases the solubility of CO_2. Therefore, overestimation of the dissolved CO_2 in water is expected in this model formulation. We are currently implementing brine in these algorithms, but we do not expect our fundamental results (different EOS algorithms will predict different migration rates and patterns) to change.

References

Abel, P. A. 2005. Investigation of subsurface CO_2 sequestration: CO_2 plume fringe mineralization. Master thesis, New Mexico Institute of Mining and Technology.

Angus, S., Armstrong, B., de Reuck, K. M., 1976, Thermodynamic Tables of the Fluid State: Carbon Dioxide. Pergamon, Oxford.

Bachu, S., 2000. Sequestration of CO_2 in geological media: criteria and approach for site selection in response to climate change, Energy Conversion and Management 41, 953-970.

Cole, B. S. 2000. An equation of state for multiphase CO_2 and water. Master thesis, New Mexico Institute of Mining and Technology.

Diamond, L. W., Akinfiev, N. N., 2003. Solubility of CO_2 in water from -1.5 to 100°C and from 0.1 to 100MPa: Evaluation of literature data and thermodynamic modeling. Fluid Phase Equilibria 208, 265-290.

Duan, Z. and Sun, R. 2003. An improvement model calculating CO_2 solubility in pure water and aqueous NaCl solutions from 273 to 533 K and from 0 to 2000 bar. Chemical Geology, v.193, 257-271.

Garcıa, J. E., 2003. Fluid dynamics of carbon dioxide disposal into saline aquifers. Ph.D Thesis, University of California, Berkeley, 136pp.

Hitchon, B. 1996. Aquifer disposal of carbon dioxide. Geoscience Publishing, Ltd, Sherwood Park, Alberta, Canada.

International Formulation Committee, 1967. A formulation of the thermodynamic properties of ordinary water substance, IFC Secretariat, Dusseldorf, Germany.

Kerrick D.M., Jacobs, G.K., 1981. A modifed Redlich-Kwong equation for H_2O, CO_2, and H_2O-CO_2 mixtures at elevated pressures and temperatures. American journal of science, v.281, 753-767.

Krumhansl, J.L., et al., 2002. Geological Sequestration of Carbon Dioxide in a Depleted Oil Reservoir. In Proceedings of the SPE/DOE 13th Symposium on Improved Oil Recovery, Tulsa, OK, April 13-17.

Law D.H.S, Bachu S. 1996. Hydrogeological and numerical analysis of CO_2 disposal in deep aquifers in the Alberta sedimentary basin. Energy Conversion& Management, vol.37, 1167-1174.

Orr, Jr.F.M., 2004. Storage of carbon dioxide in geologic formation. SPE (Distinguished lecture series).

Pawar, R.J., N.R. Warpinski, B. Stubbs, and D. Zhang, 2003. Numerical Modeling of CO_2 Sequestration In A Depleted Oil Reservoir. Proceedings of the 3rd Annual Conference on Carbon Sequestration, May 3-6, Alexandria, Virginia.

Parker, J.C., Lenhard, R.J., Kuppusamy, T., 1987. A parametric model for constitutive properties governing multiphase flow in porous media, Water Resouces Research v.23, no.4, 618-624.

Pruess, K., 1991. TOUGH2-A general purpose numerical simulator for multiphase fluid and heat flow. Report LBNL29400, Lawrence Berkeley National Laboratory, Berkeley, CA.

Reid, R.C., Prausnitz, J.M., Poling, B.E., 1987. The properties of gases and liquids. 4th edition, McGraw-Hill, Inc., New York.

Rutqvist, J., Tsang, C.F., 2002. A study of caprock hydromechanical changes associated with CO_2 injection into a brine formation.

Saripalli, K.P., Sharma, M.M., Bryant, S.L., 2000. Modeling injection well performance during deep-well injection of liquid wastes. Journal of Hydrology, v.227, 41-55.

Span, R., Wager, W., 1996. A new equation of state for carbon dioxide covering the fluid region from the triple-point temperature to 1100 K at pressures up to 800 MPa. Journal of physical chemical reference data, v.25, no.6, 1509-1596.

Spycher, N., Pruess, K., Ennis-King, J., 2003. CO_2-H_2O mixtures in the geological sequestration of CO_2. I. Assessment and calculation of mutual solubilities from 12 to 100 °C and up to 600 bar. Geochimica et Cosmochimica Acta 67 (16), 3015-3031.

Vesovic, V., Wakeham, W.A., Olchowy, G.A., Sengers, J.V., Watson, J.T.R., Millat, J., 1990. The transport properties of carbon dioxide. Journal of physical chemical reference data, v.19, no.3, 763-808.

Weir, G.J., White, S.P., Kissling, W.M., 1996. Revervoir storage and containment of greenhouse gases. Transport in porous media, v.23, 37-60.

Xu, T., Ontoy, Y., Molling, P, Spycher, N., Parini, M., Pruess, K., 2004. Reactive transport modeling of injection well scaling and acidizing at Tiwi field, Philippines. Geothermics, v.33, 477-491.